Drivers of Rh and Pt variability in the water column of a hydrodynamic estuary: effects of contrasting environments

Carlos E. Monteiro[1,2]*, Antonio Cobelo-García[3], Margarida Correia dos Santos[1] and Miguel Caetano[2]

[1] Environmental Biogeochemistry, Centro de Química Estrutural, IST-UL, Lisboa, PORTUGAL.

[2] IPMA – Instituto Português do Mar e da Atmosfera, Algés, PORTUGAL.

[3] Bioxeoquímica Mariña, Instituto de Investigacións Mariñas IIM–CSIC, Vigo, SPAIN.

*Corresponding author: carlos.e.monteiro@tecnico.ulisboa.pt

Abstract

Rhodium and platinum are among the less studied elements in estuarine waters and the understanding of their speciation analysis and environmental fate remains limited. In this study, we address the occurrence and discrimination of soluble/insoluble Rh and Pt species in aquatic systems, as well as their potential transport. Particulate and dissolved (<0.45 µm) rhodium (Rh_P and Rh_D) and platinum (Pt_P and Pt_D), respectively, were determined in the water column of contrasting environments during neap (NT) and spring (ST) tide semi-diurnal cycles: in the upper Tagus estuary (VFX) and near the mouth, close to a wastewater treatment plant outfall (ALC). Both elements were analyzed by AdCSV and ICP-MS, as well as auxiliary parameters were determined. Concentrations of Rh and Pt followed the tidal regime, presenting higher concentrations during low tide. Concentrations of Rh_P (0.1–5.1 ng g^{-1}) and Rh_D (0.03–0.12 ng L^{-1}) were lower than Pt_P (1.0–25.6 ng g^{-1}) and Pt_D (0.1–11.7 ng L^{-1}), respectively. Concentrations found in ALC were higher than VFX, except for Rh_D, mirroring anthropogenic inputs attributed to automotive catalytic converters and an additional Pt source originated in Pt-based compounds. Distribution coefficients (K_D) of 10^4 were computed and were independent of the salinity gradient. The speciation analysis done at VFX during NT showed that truly dissolved forms measured by AdCSV represented 39±9 % of total Pt in the water column, while total filter-passing species measured by ICP-MS were higher, 65±14 %. Pt speciation was controlled by its dissolved forms, whereas particulate Rh forms represented the bulk value (>65 %). The potential transport evaluated at downstream station indicated recirculation within the estuary and export towards the Atlantic Ocean, with higher concentrations associated with the ebb opposing to the flood. These results show estuaries as important pathways to introduce PGE in coastal regions, transferring them towards the ocean.

Keywords

Platinum-group elements; Aquatic systems; Particle-water interactions; Speciation analysis; Environmental fate

1. Introduction

Concentrations of platinum-group elements (PGE), such as rhodium (Rh) and platinum (Pt) have steadily increased in the environment over the past years despite their low abundance in Earth's crust (<0.5 ng g^{-1}; Peucker-Ehrenbrink and Jahn 2001; Taylor and McLennan 1995). The main anthropogenic sources of Rh and Pt originate in industrial catalysts and exhaust fumes of automotive catalytic converters (ACC) that release both elements into the environment. Moreover, Pt has also medicinal uses in anticancer drugs (Brito et al. 2020; Ek et al. 2004; Pawlak et al. 2014; Ravindra et al. 2004). The rising use of Rh and Pt led to an increase of their concentrations in different environmental compartments (Brito et al. 2020). Anthropogenic emissions released in urban environments have impacts in aquatic systems (e.g. Ek et al. 2004; Monteiro et al. 2019), consequently reflecting their transport from continental urban areas to the nearby aquatic systems. In general, concentrations of Rh and Pt in estuaries have been reported to be similar (Abdou et al. 2020a; Cobelo-García et al. 2011, 2013, 2014) or higher (Monteiro et al. 2019) than in coastal areas (Abdou et al. 2020a; Mashio et al. 2017; Obata et al. 2006), and the open ocean (Colodner 1991; López-Sánchez et al. 2019). Relatively high signatures of Rh have been found in sediments (Almécija et al. 2016; Essumang et al. 2008; Monteiro et al. 2019). The same has been found for Pt in sediments (Cobelo-García et al. 2013, 2014; Monteiro et al. 2019; Zhong et al. 2012), suspended particulate matter (SPM; Abdou et al. 2020b; Cobelo-García et al. 2013, 2014), and phytoplankton (Abdou et al. 2020a). While dissolved Pt has also been reported in the water column (Cobelo-García et al. 2013, 2014; López-Sánchez et al. 2019; Mashio et al. 2016; Obata et al. 2006; Suzuki et al. 2014), dissolved Rh concentrations in the aquatic environment (Bertine et al. 1993), and in wastewaters as well (Monteiro et al. 2017), remain very limited. Therefore, their occurrence,

distribution, mobility, and partitioning in the water column, as well as their fate in estuarine and marine environments, remain dimly elucidated.

Limited information exists about the speciation of Pt and particularly Rh in aquatic media. Regarding the dissolved forms, Rh inorganic speciation appears to be dominated by aquo-hydroxo, aquo-chloro and mixed aquo-hydroxo-chloro complexes (Bertine et al. 1996; Cobelo-García et al. 2008). As to Pt, it has been suggested that Pt(II) predominates in freshwaters, as $Pt(OH)_2$, while Pt(IV) dominates in seawater as $PtCl_5(OH)^{2-}$ (Cobelo-García et al. 2013, 2014; Mashio et al. 2017). Simultaneously, there is a need for suitable techniques that are adequately sensitive and selective to deal with speciation analysis schemes that discriminate between particulate and dissolved fractions in aquatic environments (Burden et al. 2002). A problem may arise from the different cut-off used in the separation of both fractions, i.e. either 0.2 μm filters (e.g. Cobelo-García et al. 2013, 2014) or 0.45 μm filters (e.g. Mashio et al. 2016) are currently used, enhancing the difficulty of comparing data sets. Furthermore, the operationally dissolved fraction *per se* (<0.45 μm) includes species such as colloids, with sizes varying from 1 to 1000 nm (Wilkinson and Lead 2007), and nanoparticles <100 nm as well (Adlim et al. 2009), whose mobility and bioavailability may be different from truly dissolved species (Guo and Santschi 2007; Monteiro et al. 2020). Further investigation is needed to increase the understanding on biogeochemical processes of Rh and Pt forms in waters. However, limitations still exist for Pd, and thus, it was not considered in this work.

The discrimination of soluble/insoluble Rh and Pt species in environmental samples is challenging; however, this is done here. We hypothesized Rh and Pt could be determined in the Tagus estuary water column, and the controlling fraction for each element could be inferred through a speciation scheme. Additionally, the estuarine

hydrodynamic effect on the spread and environmental fate of Rh and Pt is poorly documented. Thus, this work aims at (1) evaluating Rh and Pt physicochemical interactions and behaviour in the water column of a hydrodynamic estuary considering a salinity gradient; (2) quantifying dissolved and particulate Rh and Pt in (a) the upper part of the Tagus Estuary, nearly to the river mouth, and (b) the receptor medium of a wastewater treatment plant (WWTP) effluent in the lower Tagus Estuary (high salinity); and (3) the potential exchanges of Rh and Pt between the estuary and the Atlantic Ocean were also investigated.

2. Material and methods

2.1. Description of the study area and sampling stations

The Tagus Estuary is one of the largest estuaries in SW Europe, having an area of *ca.* 320 km^2 connected to the Atlantic Ocean (Fig. 1; Fortunato et al. 1999; Guerreiro et al. 2015; Vale and Sundby 1987). The Tagus River is the main source of freshwater to the estuary, on average 350 m^3 s^{-1}, while other small tributaries have minor contributions (<50 m^3 s^{-1}) (Fortunato et al. 1999; Guerreiro et al. 2015; Vale and Sundby 1987). Salinity variations in the estuary depend on the input of freshwater, thus, the main drive controlling the mixing process is the tide (de Pablo et al. 2019). The tidal regime of the Tagus Estuary is mainly semi-diurnal, ranging from 0.8 m (neap tide) to 4.0 m (spring tide) (Fortunato et al. 1997; Neves 2010). The tidal wave is asymmetric and progressive, causing delays up to two hours between the estuary mouth (Lisbon) and upstream locations (Vila Franca de Xira; Neves 2010; Vale and Sundby 1987). Typically, ebbs are shorter than floods (Fortunato et al. 1999; Guerreiro et al. 2015; Vaz and Dias 2014), which mirrors the stronger current velocities during ebbs (Vaz and Dias 2014). Currents near the surface can be higher than 1.5 m s^{-1} during spring tides in the lower estuary inlet (Neves 2010). Residence times within the Tagus Estuary may vary,

ranging between <10 days in the inlet channel and >20 days in the shallow bay (Braunschweig et al. 2003).

The two sampling areas are ~35 km distant one from another and present different characteristics (Fig. 1). The upstream sampling station (VFX; 38º57'4.49" N; 8º59'5.48" W; Fig. 1) is located near the entrance of the estuary. This region is less populated, served by a low dimension WWTP and is crossed by a bridge. Freshwater is the main source of water in this site, but an increase in salinity is observed due to tidal influence mainly during the high tides of spring tides. In opposition, the downstream sampling station (ALC; 38º41'53.9" N; 9º10'33.5" W; Fig. 1) is located at the vicinity of a WWTP outfall, closer to the estuary mouth, and therefore, near the Atlantic Ocean. Thus, estuarine waters in this station present higher salinity. This WWTP is one of the largest in Portugal and receives waste- and drainage waters from three municipalities in the Lisbon region that serves near 1 million persons (Marques da Costa 2016). The drainage includes domestic and hospital effluents that may contain Pt-based compounds used in cancer treatments and pluvial runoff that may have Rh and Pt from ACC. In addition, a high traffic impacted bridge crosses the inlet, where *ca*. 150,000 vehicles pass every day (IMT 2016).

2.2. Field campaigns, sampling and *in situ* measurements

Two field campaigns were carried out at each sampling station, during neap tide (NT) in June 2017 and spring tide (ST) in September 2017 covering semi-diurnal tidal cycles (12.5 h). Water samples were collected on-board of a semi-rigid vessel on an hourly basis. At VFX station two depths were considered. The surface sample was collected at ~0.5 m depth and the bottom sample was collected ~0.5 m above the riverbed. Due to shallowness of the water column at ALC station (<3 m), water was sampled only at an intermediate depth. Collection of water samples was performed

using a 5 L horizontal Niskin bottle and stored in acid-washed 2.5 L PP bottles until filtration (<2 h). Additional parameters, namely temperature (ºC), conductivity (mS cm^{-1}), pH, dissolved oxygen (DO) concentration (mg L^{-1}) and saturation (%DO), were measured *in situ* using a portable multi-parametric probe (YSI 600 QS) coupled to previously calibrated electrodes.

2.3. Analytical procedures

All laboratory procedures were executed in acclimatized conditions (25±2 ºC) using previously acid-cleaned material by immersion in ~20% both nitric acid (HNO_3) and hydrochloric acid (HCl) baths, for 48 h each. The necessary reagents for digestion and analysis of the samples were of high-purity grade. All solutions were prepared with ultra-pure water from a Milli-Q (Millipore) purification system (conductivity of 18.2 MΩ.cm).

Water samples were immediately filtered using acid-washed filtration kits coupled to kitasato flasks under low-pressure vacuum. Pre-weighted polycarbonate membrane filters (0.45 µm; Whatman Nuclepore) were used in the separation of particulate and dissolved operationally defined phases. As to the particulate fraction of the metals (Rh_P and Pt_P) and SPM (mg L^{-1}), triplicate samples were obtained. Filters were dried in an oven at 40 ºC until constant weight. The SPM was calculated by the difference of dry weight (dw; 0.01–0.03 g in average) and corrected for the filtered volume (0.1–0.5 L). Then, the filters were acid-digested in *aqua regia* at 195 ºC for the Rh_P and Pt_P determinations, as previously described in Monteiro et al (2017). For the dissolved Rh and Pt concentrations (Rh_D and Pt_D, respectively), filtrates were immediately acidified with HCl 30 % to pH <2 and preserved cold in the dark. Prior to the analysis, filtered samples were UV-irradiated in quartz tubes for 3 h, adding small volumes of H_2O_2 to

facilitate the organic matter mineralization (Cobelo-García et al. 2013; Monteiro et al. 2020). All procedure was done in triplicate, at minimum. The determination of Rh and Pt was carried out using adsorptive cathodic stripping voltammetry (AdCSV) following the procedure optimized and detailed in Monteiro et al. (2017).

The samples of VFX corresponding to NT cycle were also analysed by inductively coupled plasma–mass spectrometry (ICP-MS, Agilent 7900 equipment) for total concentrations of Rh and Pt in the filtrates ($Rh_{D\text{-}ICP\text{-}MS}$ and $Pt_{D\text{-}ICP\text{-}MS}$). Interferences of Cu ($^{63}Cu^{40}Ar^{+}$), Pb ($^{206}Pb^{2+}$), Sr ($^{87}Sr^{16}O^{+}$), Rb ($^{87}Rb^{16}O^{+}$) and Zn ($^{67}Zn^{36}Ar^{+}$) on ^{103}Rh and Hf ($^{179}Hf^{16}O^{+}$) on ^{195}Pt, and were monitored and mathematically corrected for each sample using interference ratios derived from single-metal solutions. However, interferences were significant for Rh and thus $Rh_{D\text{-}ICP\text{-}MS}$ could not be determined. It was observed that the Hf interference on Pt signal was negligible (<0.1 %). The used operating conditions are shown in supporting information (S.I.) Table S1. The relative standard deviation of repeated measurements for Pt was in general <10 %.

Dissolved organic carbon (DOC, mg C L^{-1}) was also determined in VFX samples of NT cycle. Determinations were done by wet chemical oxidation with persulfate method using an OI Analytical TOC Analyzer.

2.4. Quality control of the analytical procedures

Blanks and certified reference material (CRM BCR-723) were used to control the quality of all analytical procedures. Due to lack of CRM for Rh and Pt in waters, the accuracy of the analysis was checked by means of spiked samples (membrane filters and sampled waters) using known nominal concentrations of Rh and Pt. Briefly, mean recoveries were in general higher than 90 % and RSD below 15 %. The limits of detection (LOD) of AdCSV analysis obtained for the water samples using a deposition

time of 300 s were 0.03 ng Rh L^{-1} and 0.06 ng Pt L^{-1}. For the total concentrations in the acid-digested solids, using deposition time of 120 s, LOD were 0.1 ng Rh L^{-1} and 0.2 ng Pt L^{-1} using typically 0.02 g of sample (dw). No cross-contamination was observed. The LOD determined for $Pt_{D\text{-}ICP\text{-}MS}$ analysis was 0.05 ng L^{-1}.

2.5. Tidal conditions and current velocity data acquisition

Tidal heights (m) and current velocities (m s^{-1}) at each station were obtained from the hydrodynamic model MOHID (Neves 1985). The tidal heights were obtained from the tidal gauge located in the Tagus Estuary (Lisbon harbour – LTG; 38.71ºN and –9.13ºW), provided by the Portuguese Hydrographic Institute. Current velocities were acquired after forcing the model, previously calibrated and validated (de Pablo et al. 2019), for the periods of interest and the components of current velocities were retrieved at each sampling site on an hourly basis.

2.6. Statistical analysis

The software Statistica (v.12) was used to check the data for outliers using Grubbs test and for normality using the Kolmogorov-Smirnov & Lilliefors tests. One or more variables presented non-normal distribution and subsequent analysis was carried out using non-parametric statistics. Spearman correlations (R_S) were used for paired-wise multiple comparison of variables. The minimum level of confidence used was 95 %. Principal component analysis (PCA) was applied to evaluate and discriminate which group of variables explained the highest variance of the results (Miller and Miller 2010).

3. Results

3.1. Variability of Rh and Pt concentrations in the upstream site VFX

The physicochemical water properties at VFX site during the semi-diurnal tidal cycles, at neap tide (NT) and spring tide (ST), are presented in S.I. Fig. S1 and S2. In general, the variations observed in the water properties reflected the tidal semi-diurnal (high and low tides) and the fortnightly oscillations, i.e. there was a trend in the parameters to increase during the flood and to decrease in the ebb tides. Minor variations observed between both depths reflected the mixture of the water column. Despite the tidal influence, no significant changes ($p > 0.05$) were found between the two depths on each of the tidal cycles.

The concentrations of particulate Pt (Pt_P) and Rh (Rh_P) in surface and bottom layers of the water column, for both tidal cycles at VFX station, are shown in Fig. 2a. Concentrations of Pt_P varied between 1.0 and 11.3 ng Pt g^{-1} in NT, and between 2.7 and 11.3 ng Pt g^{-1} in ST. Similarly, concentrations of Rh_P varied within one order of magnitude, between 0.1 and 2.0 ng Rh g^{-1} in NT, and between 0.2 and 1.8 ng Rh g^{-1} in ST. In both campaigns, Pt_P concentrations were higher than Rh_P. The erratic variation for both Pt_P and Rh_P in the NT cycle was not observed in ST, where maximum concentrations were measured between 18:00 and 19:00 following the increase exhibited in conductivity and pH (S.I. Fig. S1). Dissolved metal concentrations measured by AdCSV, Pt_D and Rh_D, in surface and bottom layers of the water column for both tidal cycles at VFX station are presented in Fig. 2b. Concentrations of Pt_D varied between 0.18 and 0.43 ng Pt L^{-1} in NT and between 0.12 and 0.73 ng Pt L^{-1} in ST. While in NT Pt_D was relatively constant, two increments were observed in ST cycle, at 12:00 and 16:00. The first peak was coincident with low tide while the second one occurred during the flood. As to Rh_D in NT, concentrations were below 0.03 ng Rh L^{-1}

(LOD). The exception was observed in the bottom water, 0.05 ng Rh L^{-1}, between 9:00 and 10:00, which was closer to high tide. Contrastingly, Rh_D in ST increased almost one order of magnitude, between the LOD and 0.19 ng Rh L^{-1}. Increments of Rh_D were also found in the low tide, at 12:00, and during the flood period with the maximum value at 16:00, similarly to Pt.

The total concentrations of Pt in the filtrates (<0.45 μm) were also determined by ICP-MS ($Pt_{D\text{-}ICP\text{-}MS}$) in the samples with low conductivity (in average 1 mS cm^{-1}), i.e. in the NT cycle of VFX. Rhodium in the same samples could not be measured due to the very low concentrations and the large polyatomic interferences to its determination (Cu, Pb, Sr, Rb). In Fig. 3, Pt measured in the filtrates by AdCSV and ICP-MS is shown. Concentrations of $Pt_{D\text{-}ICP\text{-}MS}$ ranged from 0.34 to 0.42 ng Pt L^{-1} in surface and from 0.33 to 0.58 ng Pt L^{-1} in the bottom. For both depths, $Pt_{D\text{-}ICP\text{-}MS}$ was higher than Pt_D. Similar variation patterns along the tidal cycle can be considered for both $Pt_{D\text{-}ICP\text{-}MS}$ and Pt_D, yet differences were observed at the bottom from 7:00 until 12:00.

In spite of no significant differences ($p>0.05$) found on the water properties between depths for both NT and ST cycles, metals and their relationships with the water properties in the different cycles were evaluated combining both depths. The principal component analysis (PCA) is shown in S.I. Fig. S3 and the tables of correlation for NT and ST are presented in S.I. Tables S2 and S3, respectively.

3.2. Variability of Rh and Pt concentrations in the downstream site ALC

The physicochemical water properties of the intermediate depth sampled at ALC site during NT and ST are presented in S.I. Fig. S4. In general, data analysis of the sampled temporal series showed good agreement between the measured variables and tidal

oscillation. Considering the location at the discharge of a WWTP, the minor variations observed on some of the variables were due to the input of wastewater.

The concentrations of particulate (Pt_P and Rh_P) and dissolved (Pt_D and Rh_D) metals in the water column for both tidal cycles at ALC station are shown in Fig. 4. Concentrations of Pt_P varied from 2.0 to 25.6 ng Pt g^{-1} in NT and from 4.2 to 22.1 ng Pt g^{-1} in ST. Values in the dissolved fraction also ranged within an order of magnitude, between 0.2 and 5.3 ng Pt L^{-1} in NT, and between 0.2 and 11.7 ng Pt L^{-1} in ST. Both particulate and dissolved fractions of Pt presented a similar variation pattern, with the highest concentrations at low tides. In addition, a relative increase of both Pt_P and Pt_D concentrations occurred at ~10:00 and ~18:00 during the NT campaign. The same increase on both periods of the day was also observed in ST, however, those coincided with the tidal dynamics (low and high tide, respectively). Concentrations of Rh_P varied from 0.3 to 5.1 ng Rh g^{-1} in NT and from 0.2 to 4.3 ng Rh g^{-1} in ST. Small peak concentrations of Rh_P were observed in the NT around 10:00 and a maximum at ~16:00. For the same periods of the day, at 9:00 and 17:00, increments were similarly found in the ST. As to Rh_D concentrations in both cycles, these ranged from LOD to 0.12 ng Rh L^{-1}. The variation pattern displayed by Rh_P did not appear to follow the tidal dynamics, as opposed to Rh_D that in general presented the highest concentrations in low tides of NT and ST.

The PCA is shown in S.I. Fig. S5 and the main relationships found between Pt, Rh and the water parameters at ALC are shown in S.I. Fig. S6. The corresponding correlations for NT and ST are presented in S.I. Tables S4 and S5, respectively.

3.3. Geographical inter-comparison

3.3.1. Particle-water distribution coefficients (K_D)

The distribution coefficients, K_D (L g^{-1}) (e.g. Sung 1995; Tessier 2019), were evaluated along the conductivity gradient of both campaigns and are presented in Fig. 5a. Including both tidal cycles, the Log transformations of K_D (Fig. 5b) for Pt ranged from 3.2 to 5.0 at ALC, and from 3.4 to 4.6 at VFX. Similarly, Log K_D for Rh varied from 3.2 to 5.3 at ALC, and from 3.0 to 4.7 at VFX. No significant differences differences ($p>0.05$) were found for both metals amongst sites.

3.3.2. PCA

In Fig. 6 is presented the PCA for all data monitored in the Tagus Estuary. Two principal components (PC) were extracted and together explained 64.9 % of the variance. The first component, PC1, described 40.9 %. It is noticeable that PC1 separated both locations monitored in the estuary, most likely relating the salinity gradient. This is best described by the water characteristics, the conductivity in particular, that differ in downstream station ALC, near to the Atlantic Ocean, from the upstream station VFX. The second component, PC2, accounted for 23.9 % of the explained variance. This component appeared to be associated with the semi-diurnal tidal regime. Noteworthy in the ALC station, the separation displayed between low and high tides evidenced the effect of PC2. The same was observed at VFX station during ST cycle; however, with a fewer number of scores. In addition to the tidal regime, pH was exhibited as the main driver controlling PC2, associated to the semi-diurnal regime. Nevertheless, the loadings had relevant distribution in the four quadrants of the PCA, evidencing their weight on both components.

3.4. Estuarine and coastal exchanges of Rh and Pt

The potential exchanges of Rh and Pt between the Tagus Estuary and the Atlantic Ocean were evaluated using the data from the downstream station ALC (Fig. 1). Initially, the concentrations of metals were projected against the corresponding horizontal component (u) of the current velocity field obtained from the hydrodynamic model MOHID (Fig. 7). Considering only current velocities higher than 0.75 m s^{-1}, differences were observed amongst the tides. Both fractions of Rh and Pt were particularly associated with the highest currents during the ebb tide, towards the Atlantic Ocean, as opposed to those during the flood. This was less pronounced towards the inner estuary, however, pointing out recirculation in the inner bay. The exception was Rh_D that presented similar range of concentrations in both ebb and flood tides during ST.

4. Discussion

4.1. Environmental and hydrographic context

Variations of ancillary parameters at both sites followed the tidal regime, as well as the inputs of fresh- or wastewaters to the estuary from VFX and ALC, respectively. At VFX station, surface and bottom layers presented similar characteristics in both tidal cycles, indicating that the water column was in general uniform and well mixed. Differences displayed between tidal cycles at VFX in some ancillary parameters indicated the extent of the tidal effect, also evidenced by the PCA (Fig. S3). Conductivity (Fig. S2) was higher in ST than in NT, owing to the stronger upward movement of the tidal wave under this condition. The temperature of the waters showed an opposite trend to the tidal influence. Regardless the small variation in the temperature range, it could be seen that the entrance of freshwater to the estuary

responded to the semi-diurnal oscillation. In ST, variations of pH closely followed the increase of conductivity and thus the tidal regime (Fig. S2).

In the downstream station ALC, the tidal amplitude is larger than at VFX. Even so, the effect of the tidal regime in the water properties is less pronounced than VFX due to the proximity to the Atlantic Ocean. Thus, the physicochemical characteristics of the water at ALC did not vary considerably between tidal cycles but followed the semi-diurnal tidal regime, as also confirmed by the PCA (Fig. S5). During low tides, the effluent discharge of the WWTP to the estuary was more detectable, owing to the shallower water column. This was clear by the maximum values of temperature recorded in the low tide during both NT and ST campaigns. Accordingly, a decrease in the conductivity and pH was found, as opposed to those rises in temperature (S.I. Fig. S4). Despite similar range on SPM levels found in both stations, relatively small increments were observed during low tides. Concentrations of suspended particulate matter SPM found in the Tagus Estuary during these campaigns indicated low turbidity in the water column in both sites as compared to other large estuaries (e.g. the Gironde; e.g. Cobelo-García et al. 2014).

The Tagus Estuary is an ebb-dominated mesotidal system with fortnightly oscillations and depends on the mixture of riverine and coastal waters. A salinity gradient was observed between both locations and tidal cycles, mainly at VFX during ST. Vertical stratification of the water column did not occur due to bottom topography and tidal oscillation. The extent of the tidal wave can reach up to 50 km upstream (Guerreiro et al. 2015), passing upward VFX station, but the tidal amplitude is less pronounced at VFX than in ALC. In addition, it was observed particularly for VFX tidal cycles some gap between the physicochemical parameters data and the tidal height,

given by the hydrodynamic model MOHID. This may be explained by the delay on the propagation of the tidal wave up to ~2 h from the mouth up to VFX.

4.2. Concentrations and physicochemical characterization of Rh and Pt

Particulate concentrations recorded during both tidal cycles ranged from 1.0 to 11.3 ng Pt g^{-1} at VFX, and up to 25.6 ng Pt g^{-1} at ALC. These values are in line with the levels reported for other estuaries, such as the Lérez (2.1–8.0 ng Pt g^{-1}, Cobelo-García et al. 2013), yet higher than those reported for the Gironde (0.2–1.8 ng Pt g^{-1}, e.g. Cobelo-García et al. 2014). As to Rh_P, low concentrations were observed, ranging from 0.1 to 2.0 ng Rh g^{-1} at VFX and from 0.2 to 5.1 ng Rh g^{-1} at ALC. To our knowledge, data on Rh_P in water column of aquatic systems are not available. Consequently, comparison can only be done with matrices like sediments and road dusts, which may represent the closest approximation to SPM. Rhodium concentrations measured in SPM were relatively higher than those found in superficial sediments of the Tagus Estuary (0.02–1.5 ng Rh g^{-1}; Monteiro et al. 2019) and much lower than those reported by Monteiro et al. (2020) for an urban road dust (44 ng Rh g^{-1}).

As to the dissolved fraction, Pt_D ranged up to 0.73 ng Pt L^{-1} near the river mouth (VFX) and up to 11.7 ng Pt L^{-1} at the WWTP outfall (ALC). Cobelo-García et al. (2013) reported lower concentrations for the Lérez river estuary in Pontevedra Ria, Spain, with Pt_D ranging between 0.01 and 0.12 ng L^{-1}. Mashio et al. (2016) also reported in Arakawa, Kotsuchi and Otsuchi rivers, Japan, Pt_D ranging up to 1.3 ng L^{-1}. For the low to medium-salinity range in the waters sampled by those authors, the Pt_D levels found at VFX are comparable to those findings. Moreover, Obata et al. (2006) found in Tama river, Japan, increased concentrations of Pt_D varying up to 6.9 ng Pt L^{-1} that, although higher, did not reach the values found at ALC station. While in the river end-member Rh_D was often below 0.03 ng Rh L^{-1} (LOD), at the WWTP discharge site Rh_D reached

0.12 ng Rh L^{-1} in both tidal cycles. To date, the only data on Rh_D was reported for the open ocean by Bertine et al. (1993), whose concentrations were <0.1 ng Rh L^{-1}, and more recently by Monteiro et al. (2017) in wastewaters, whose average concentration was 0.23±0.06 ng Rh L^{-1}.

In general, Pt concentrations in both fractions were higher than Rh for the two sites sampled. At VFX station, Pt_P and Rh_P were lower compared to the downstream station ALC that was influenced by the discharge of the WWTP. As with the particulate fraction, Pt_D and Rh_D were also lower at VFX compared to ALC. These results point out spatial differences on the anthropogenic loadings of Rh and Pt to the Tagus Estuary. The direct point sources derived from ACC at VFX where the main sources are a low-traffic influenced bridge and the drainage basin that covers largely rural areas. At ALC, the WWTP converges pluvial and sewage waste from a large drainage urban basin, which includes three municipalities from the most densely populated part of Lisbon region. During both campaigns at ALC, increased concentrations of both Pt_P and Pt_D (Fig. 4) were recorded in the morning (~10:00) and afternoon (~18:00) periods. This suggests added Pt levels in the effluent of the WWTP (Kümmerer et al. 1999; Laschka and Nachtwey 1997; Vyas et al. 2014), most likely deriving from Pt-based anticancer compounds (Kümmerer et al. 1999; Vyas et al. 2014). Degradation in the environment could release Pt aqueous species (Curtis et al. 2010), presumably detectable by the voltammetric method used because of the high doses administered to patients in chemotherapy (e.g. 200–500 mg cisplatin L^{-1}; www.infarmed.pt). Since Pt-based drugs are mainly excreted in urine (Oun et al. 2018), those peaks can be related cancer treatment. The Pt/Rh mass ratios (S.I. Table S6) calculated for NT and ST cycles support previous observations. At VFX, including both campaigns, the particulate Pt/Rh was primarily within the range typically found for ACC emissions (4-16; Rauch and

Peucker-Ehrenbrink 2015). At ALC, higher Pt/Rh mass ratios (up to 69) contrasted with those found at VFX, largely exceeding the reference interval for ACC, especially in ST. Furthermore, the elevated Pt/Rh mass ratios were observed during low tides of both cycles that is likely due the lesser dilution of the effluent discharge in the estuary as opposed to the high tides. When using the dissolved fraction of the metals, the calculated mass ratios were slightly higher than in particulate fraction, yet following the same trend. Therefore, concentrations found in the water column of the Tagus Estuary reflected the different sources and contributions at both sites.

While irregular short-term variations of Pt_P and Rh_P were exhibited at VFX during NT, notwithstanding the tidal regime, the opposite was observed during ST at VFX and in both of ALC tidal cycles. The increase on Pt_P and Rh_P at VFX during ST (Fig. 2a) appeared to follow the semi-diurnal variation during the high tide (≈18:00). In surface, Pt_P increased with the conductivity and pH (Fig. S1), as expressed by the significant correlations (S.I. Tables S2 and S3) found in NT (R_S=0.518; p<0.05; n=26) and ST (R_S=0.448; p<0.05; n=26). Despite this signal was observed in a period of ~2 h concurrent to the high tide peak, this observation may be explained by the existence of a downstream bridge (within 20 km distance) largely impacted by vehicles traffic. In fact, Monteiro et al. (2019) observed in superficial sediments a signal of both Rh and Pt that pointed out large emissions from ACC. Those particles once in the surface of the water column may be transported during the flood tide up to VFX. As to ALC, Rh and Pt (Fig. 4) closely followed the temperature short-term variation and showed an opposing trend to conductivity (S.I. Fig S4), reflecting the characteristics of the inputted sewage. The strong positive correlation found during NT (S.I. Table S4) for Pt with the temperature (R_S=0.835; p<0.0001; n=13; S.I. Fig. S6b) as opposed to those found with the estuarine water characteristics (e.g. the conductivity, R_S=-0.885; p<0.0001; n=13; S.I. Fig. S6a)

support the WWTP as one of the main pathways of Pt entrance in the Tagus Estuary. This distinct pattern may be easily explained by the water column shallowness, in addition to the impact of direct discharge of the WWTP effluent. These results evidence a close relationship between the semi-diurnal tidal oscillations, and the source inputs of both metals to the estuary, also evidenced in PCA of ALC data (S.I. Fig. S6).

4.3. Particle-water interactions of Rh and Pt

The distribution coefficients, K_D (L kg^{-1}) can give some information about the affinity of Rh and Pt for the particulate phase in an aquatic matrix, and hence about their mobility (e.g. Sung 1995; Tessier 2019). Particle-water distribution coefficients did not present significant differences ($p>0.05$) amongst tidal cycles and along the salinity gradient (Fig. 5a). Consequently, no significant differences ($p>0.05$) were observed between sites and metals, as expressed by the Log transformation (Fig. 5b). Thus, median values of Log K_D can be considered for Rh and Pt in the Tagus Estuary, 4.1±0.5 (n=34) and 4.0±0.4 (n=75), respectively. Data on K_D for Rh and Pt obtained from natural settings, such as rivers or estuaries, remain very limited in the literature (e.g. Abdou et al., 2020b; Cobelo-García et al., 2008, 2013, 2014). Comparison with published data must be careful due to varying cut-off membrane filters used to discriminate phases (<0.2 or <0.45 µm). Furthermore, the relatively large colloids included in the 'dissolved' phase may also rule Rh and Pt variability/partitioning. As discussed, similar levels of SPM were measured in VFX and ALC, with an average concentration of 50 mg L^{-1}, and consequently similar K_D values could be foreseen. The K_D values found for Pt in the Tagus Estuary are in between those previously reported for other estuaries with quite different concentrations of SPM. For the Lérez, a low turbidity estuary with SPM of a few mg L^{-1}, K_D in the range of 10^5 to 10^6 were determined (Cobelo-García et al. 2013) while in Gironde, with SPM in the 100–2000

mg L^{-1}, $K_D < 10^4$ were found (Cobelo-García et al. 2014). The larger values of SPM are many times associated with larger particles that are less prone to adsorb metal ions and then the inverse relationship between SPM and K_D. The negative significant correlations observed for Pt_P with SPM in all situations corroborates the previous observations, except for ALC in the NT. Here, the different behaviour was observed most probably due to the impact of the WWTP discharge. As to the observed K_D absence of variation with salinity (Fig. 5a), it points out that the interaction with particulate matter is most likely due to neutral charge Rh and Pt, either in the metallic form or through neutral complexes. Constant K_D values along a salinity gradient were also reported for the Gironde by Cobelo-García et al. (2014). Such invariant trend, as described here for the Tagus, may also reflect the higher anthropogenic input of both fractions of Rh and Pt to the system. Different local anthropogenic pressures may also affect soluble/insoluble species during estuarine mixing (Cobelo-García et al., 2014). Therefore, Pt, at least, appears to have a non-conservative behaviour in the Tagus Estuary.

4.4. Speciation analysis of Rh and Pt in the water column

In the samples of VFX station NT cycle (Fig. 3), with average conductivity of 1 mS cm^{-1}, Pt_D and $Pt_{D\text{-}ICP\text{-}MS}$ were determined following the same methodology as in Monteiro et al. (2020). Due to operational difficulties of ICP-MS in dealing with more saline samples (conductivity >1 mS cm^{-1}, Wolf and Adams 2015), Rh and Pt speciation analysis in the water column at VFX at ST and ALC in both tidal cycles could not be done. The Pt_D and $Pt_{D\text{-}ICP\text{-}MS}$ concentrations were considerably different in all samples and no significant correlation ($p>0.05$) was found between them. Total Pt concentrations in the water column (ng L^{-1}) were computed as the sum of Pt_P (expressed in ng L^{-1}) and $Pt_{D\text{-}ICP\text{-}MS}$ (Table 1). The data of the particulate fraction (>0.45 µm) presented in ng L^{-1} took into account the mass (dw) and volume filtered of each sample,

thus no bias is expected to occur. Moreover, ICP-MS atomizes and ionizes functionally dissolved, as well as colloids and nanoparticles (Meermann and Nischwitz 2018), thus giving an approximation to the total filter-passing species (<0.45 µm). Platinum speciation analysis in these samples showed that the truly dissolved forms represented 39±9 % of the total concentrations in the water column. The percentage of total filter-passing species was 65±14 %. The differences observed are due to colloidal and/or nanoparticles forms, whether in the metallic state Pt^0 or strongly bound both to inorganic and organic colloids. As it is known, DOC can play a role in colloids aggregation/disaggregation (Wilkinson and Lead 2007), but comparable and low values were obtained in the water column, ranging 3–4 mg C L^{-1} (S.I. Fig. S2). Thus, these results suggest that DOC does not rule the aggregation/disaggregation processes in the water column, at least when low concentrations of Pt were found such as in the case of VFX station.

As to Rh, no speciation analysis could be done, because Rh_D concentrations were in general below the LOD. However, some additional considerations can be made. In all samples, truly dissolved Rh concentrations were very low, usually below LOD, and they may result from the already oxidized forms present in the water column. As to the particulate forms, the range of concentrations found, in ng L^{-1} (Table 1), were similar for both stations in NT conditions. In most of the samples, Rh_P could represent the total Rh found in the water column, since no Rh_D concentrations were found. In some cases, Rh_P was more than 65 % of the Rh_D concentrations measured. Moreover, an increase in SPM may not represent an additional input of Rh and Pt, as observed for Pt at ALC station (S.I. Fig. S6c). A contribution to the particulate pool could be the removal from the aqueous phase, by adsorption of cationic hydroxychlorides and precipitation of destabilized hydroxyl-complexes (Cobelo-García et al. 2008). However, an increase in

salinity did not change Pt and Rh partition in the water column (Fig. 5a) and higher concentrations were found for Pt_D in ALC as compared to VFX, suggesting that the dissolved forms control Pt speciation in the water column even without taking into account the additional fraction that could be measured by ICP-MS. Other sources than the ACC are present that are responsible for the increase of soluble forms of Pt into the estuary and those originate in medicinal uses of Pt-based compounds. As to Rh, these observations point out ACC as the main source of Rh into the estuary. Contrarily to Pt, Rh_P may represent an important proportion of the bulk Rh in the water column.

4.5. Hydrodynamic forcing on Rh and Pt transport

The input of Rh and Pt to the Tagus Estuary at upstream VFX station is low and continuous. In opposition, at the downstream station ALC, higher and variable concentrations of Rh and Pt enter the estuary through the WWTP output. Here, solutes and particles discharged may be widely spread by advection through the tidal currents that reach velocities closer to 1.0 m s^{-1} and may dominate the transport. As confirmed in the PCA including all the data (Fig. 6), it is noticeable the influence of the hydrodynamic and tidal regime on both locations monitored. Moreover, Rh and Pt appeared to have non-conservative behaviour in the Tagus Estuary, because of their different point sources. Non-conservative mixing was also observed in other estuaries (Cobelo-García et al. 2013, 2014).

Concerning the distribution of Rh and Pt in the water column and their fate, data from the downstream station ALC was evaluated because of the proximity to the Atlantic Ocean and the potential export to the adjacent coastal area. Higher concentrations of both fractions of Rh and Pt were released mainly during the low tide. Depicting Rh and Pt concentrations against the corresponding current velocities (Fig. 7), the export of the metals is towards the coastal area. The back and forth tidal movement

induces dispersion of particles and solutes originated from the WWTP outfall towards both the Atlantic Ocean and the inner estuary. However, their association with higher current velocities during the ebb was observed for Pt_P, Rh_P and Pt_D, whereas Rh_D had similar concentrations during both tidal periods. Thus, the probability of recirculation in the estuary, and export of Rh and Pt to the adjacent coast is very high and perhaps, occurs within a couple of days considering the residence time of the water (Braunschweig et al. 2003; de Pablo et al. 2019). Furthermore, these results suggest that part of the Rh and Pt can recirculate until, eventually, they settle in low hydrodynamic areas near the estuary margins. Monteiro et al. (2020) showed that for road dust leachates, relatively constant concentrations of truly dissolved Rh and Pt were observed up to 7 days. Nonetheless, other sources of Rh and Pt do exist in the Tagus Estuary (Monteiro et al. 2019) and further research should aim at evaluating their extension and fate.

The importance of the hydrodynamic regime at the mouth of the Tagus Estuary was previously investigated for other metals (e.g. Duarte and Caçador 2012; Vale 1986). Despite the Tagus Estuary does not appear to be extensively contaminated by Rh and Pt to date (Monteiro et al. 2019), the estuary is a net source of both metals to the coastal environment. Records of Pt were previously reported by Cobelo-García et al. (2011) in sediments of the Tagus pro-delta. The authors described a Pt enrichment in sub-surface sediments at the adjacent coastal area, owing to the extensive industrial activities in the Tagus Estuary around 1960s/70s and mimicking the records found for Hg and Pb (Mil-Homens et al. 2009). However, a superficial enrichment of Pt was not fully observed in that core despite the relative increase of Pt concentration in the top layer of those sediments. This slight increment did not reflect the anthropogenic inputs at that time, because the core was collected in 2002, one decade after the introduction of

European legislation regarding the control of pollutants emission using ACC (European Commission 1991). Thus, it is plausible that with the increase of Rh and Pt uses over the past two decades increased amounts of these metals could have been exported to the adjacent coastal area. Nevertheless, it was demonstrated that Rh and Pt are continuously released in the aquatic environment, at least evidenced through the Pt concentrations found at the downstream WWTP outfall in the Tagus Estuary.

5. Conclusions

Concentrations of particulate and dissolved fractions (<0.45 µm) of Rh and Pt were evaluated in the water column of the Tagus Estuary. Two contrasting sites were monitored during semi-diurnal cycles over neap and spring tides. Near the river mouth, both particulate Rh and Pt, as well as Pt_D, were continuously introduced in the estuary although presenting low and relatively constant concentrations, whereas Rh_D was often below the limit of detection. Contrastingly, at the downstream WWTP outfall, a marked increase was registered in both fractions of Rh and Pt. Concentrations followed an inverse pattern in relation to the semi-diurnal tidal oscillation with higher concentrations observed during the low tide. This was more pronounced at the WWTP outfall vicinity, where one of the confirmed sources of Rh and Pt was that of ACC, expressed by the concomitant variation of both metals. An additional source of Pt in the wastewater derived from hospital and domestic sewages due to the use of Pt in anticancer therapy, showing relative increments in periods that were associated with personal care activities. At the upstream station, the source of Rh and Pt is presumably mainly the ACC, though pointing to minor inputs to the estuary. The partition coefficients for Rh and Pt in the Tagus Estuary varied independently of the salinity, suggesting that the effects of Rh and Pt sources may hinder their chemical interactions with the estuarine water. The speciation analysis has confirmed that different forms of Pt were released in

the environment, whose dissolved fraction includes truly dissolved species and (nano)particles. The operationally defined forms of dissolved Pt represented the largest component of total metal emitted as opposed to Rh, that was dominated by particulate forms in the water column. Advection largely controls the distribution and rapidly dispersion through the water column of Rh and Pt owing to their low reactivity. Therefore, recirculation within the estuary and export towards the adjacent coastal environment occurs. Thus, both chemical and physical drivers control the distribution, transport and fate of Rh and Pt. Ultimately, results showed that estuaries are an important pathway by which PGE are introduced to coastal regions and transferred towards the ocean.

Acknowledgements

The Portuguese Foundation for Science and Technology (FCT) is acknowledged for the grant funding SFRH/BD/111087/2015 to CEM and the support of FCT projects PTDC/QEQ-EPR/1249/2014 - REEuse and CQE-IST projects UIDB/00100/2020 and UIDP/00100/2020 (previous funding - UID/QUI/00100/2013 and UID/QUI/00100/2019). The authors also acknowledge the COST Action TD1407 – NOTICE by means of a short term scientific mission support to CEM. The authors also gratefully acknowledge the contributions of Rute Cesário, Pedro Brito, Rui Silva, Mário Mil-Homens and Marta Nogueira during the sampling campaigns and to Hilda de Pablo for providing the hydrodynamic data from MOHID. Finally, the significant improvements of this work provided by the anonymous reviewers is gratefully acknowledged.

References

Abdou, M., Gil-Díaz, T., Schäfer, J., Catrouillet, C., Bossy, C., Dutruch, L., et al. (2020). Short-term variations of platinum concentrations in contrasting coastal environments: The role of primary producers. *Marine Chemistry*, *222*, 103782. doi:10.1016/j.marchem.2020.103782

Abdou, M., Schäfer, J., Gil-Díaz, T., Tercier-Waeber, M. Lou, Catrouillet, C., Massa, F., et al. (2020). Spatial variability and sources of platinum in a contaminated harbor-tracing coastal urban inputs. *Environmental Chemistry*, *17*(2), 105–117. doi:10.1071/EN19160

Almécija, C., Cobelo-García, A., & Santos-Echeandía, J. (2016). Improvement of the ultra-trace voltammetric determination of Rh in environmental samples using signal transformation. *Talanta*, *146*, 737–743. doi:10.1016/j.talanta.2015.06.032

Auffan, M., Rose, J., Bottero, J.-Y., Lowry, G. V, Jolivet, J.-P., & Wiesner, M. R. (2009). Towards a definition of inorganic nanoparticles from an environmental, health and safety perspective. *Nature Nanotechnology*, *4*(10), 634–641. doi:10.1038/nnano.2009.242

Bertine, K. K., Koide, M., & Goldberg, E. D. (1993). Aspects of rhodium marine chemistry. *Marine Chemistry*, *42*(3–4), 199–210. doi:10.1016/0304-4203(93)90012-D

Bertine, K. K., Koide, M., & Goldberg, E. D. (1996). Comparative marine chemistries of some trivalent metals - bismuth, rhodium and rare earth elements. *Marine Chemistry*, *53*(1–2), 89–100. doi:10.1016/0304-4203(96)00015-1

Braunschweig, F., Martins, F., Chambel, P., & Neves, R. (2003). A methodology to estimate renewal time scales in estuaries: the Tagus Estuary case. *Ocean Dynamics*, *53*(3), 137–145. doi:10.1007/s10236-003-0040-0

Brito, P. L. B. A., Cesário, R., & Monteiro, C. E. (2020). Lesser-known Metals with Potential Impacts in the Marine Environment. In *Coastal and Deep Ocean Pollution* (pp. 215–247). CRC Press. doi:10.1201/9780203704271-10

Burden, F. R., Foerstner, U., McKelvie, I. D., & Guenther, A. (2002). *Environmental Monitoring Handbook*. New York: McGraw-Hill Education.

Cobelo-García, A., López-Sánchez, D. E., Almécija, C., & Santos-Echeandía, J. (2013). Behavior of platinum during estuarine mixing (Pontevedra Ria, NW Iberian Peninsula). *Marine Chemistry*, *150*, 11–18. doi:10.1016/j.marchem.2013.01.005

Cobelo-García, A., López-Sánchez, D. E., Schäfer, J., Petit, J. C. J., Blanc, G., & Turner, A. (2014). Behavior and fluxes of Pt in the macrotidal Gironde Estuary (SW France). *Marine Chemistry*, *167*, 93–101. doi:10.1016/j.marchem.2014.07.006

Cobelo-García, A., Neira, P., Mil-Homens, M., & Caetano, M. (2011). Evaluation of the contamination of platinum in estuarine and coastal sediments (Tagus Estuary and Prodelta, Portugal). *Marine Pollution Bulletin*, *62*(3), 646–650. doi:10.1016/j.marpolbul.2010.12.018

Cobelo-García, A., Turner, A., & Millward, G. E. (2008). Fractionation and reactivity of platinum group elements during estuarine mixing. *Environmental Science and Technology*, *42*(4), 1096–1101. doi:10.1021/es0712118

Colodner, D. (1991). *The marine geochemistry of Rhenium, Iridium and Platinum*. *Massachusetts Institute of Technology*. PhD Thesis, Massachusetts Institute of Technology, USA.

Curtis, L., Turner, A., Vyas, N., & Sewell, G. (2010). Speciation and reactivity of

cisplatin in river water and seawater. *Environmental Science and Technology*, *44*(9), 3345–3350. doi:10.1021/es903620z

de Pablo, H., Sobrinho, J., Garcia, M., Campuzano, F., Juliano, M., & Neves, R. (2019). Validation of the 3D-MOHID hydrodynamic model for the Tagus coastal area. *Water (Switzerland)*, *11*(8). doi:10.3390/w11081713

Duarte, B., & Caçador, I. (2012). Particulate metal distribution in Tagus estuary (Portugal) during a flood episode. *Marine Pollution Bulletin*, *64*(10), 2109–2116. doi:10.1016/j.marpolbul.2012.07.016

Ek, K. H., Morrison, G. M., & Rauch, S. (2004). Environmental routes for platinum group elements to biological materials--a review. *The Science of the total environment*, *334–335*, 21–38. doi:10.1016/j.scitotenv.2004.04.027

Essumang, D. K., Dodoo, D. K., & Adokoh, C. K. (2008). The impact of vehicular fallout on the Pra estuary of Ghana (a case study of the impact of platinum group metals (PGMs) on the marine ecosystem). *Environmental Monitoring and Assessment*, *145*(1), 283–294. doi:10.1007/s10661-007-0037-0

European Commission. (1991). Council Directive 91/542/EEC of 1 October 1991 amending Directive 88/77/EEC on the approximation of the laws of the Member States relating to the measures to be taken against the emission of gaseous pollutants from diesel engines for use in vehicles. *OJ L 295*, 1–19 (ES, DA, DE, EL, EN, FR, IT, NL, PT).

Fortunato, A. B., Baptista, A. M., & Luettich, R. A. (1997). A three-dimensional model of tidal currents in the mouth of the Tagus estuary. *Continental Shelf Research*, *17*(14), 1689–1714. doi:10.1016/S0278-4343(97)00047-2

Fortunato, A. B., Oliveira, A., & Baptista, A. M. (1999). On the effect of tidal flats on the hydrodynamics of the Tagus estuary. *Oceanologica Acta*, *22*(1), 31–44. doi:10.1016/S0399-1784(99)80030-9

Guerreiro, M., Fortunato, A. B., Freire, P., Rilo, A., Taborda, R., Freitas, M. C., et al. (2015). Evolution of the hydrodynamics of the Tagus estuary (Portugal) in the 21st century. *Journal of Integrated Coastal Zone Management*, *15*(1), 65–80. doi:10.5894/rgci515

Guo, L., & Santschi, P. H. (2007). Ultrafiltration and its Applications to Sampling and Characterisation of Aquatic Colloids. In *Environmental Colloids and Particles: Behaviour, Separation and Characterisation* (pp. 159–221). doi:10.1002/9780470024539.ch4

IMT. (2016). *Relatório de Tráfego na Rede Nacional de Auto-estradas - 4º Trimestre de 2016*. Instituto da Mobilidade e dos Transportes, I.P., Lisboa, Portugal.

Kümmerer, K., Helmers, E., Hubner, P., Mascart, G., Milandri, M., Reinthaler, F., & Zwakenberg, M. (1999). European hospitals as a source for platinum in the environment in comparison with other sources. *Science of the Total Environment*, *225*(1–2), 155–165. doi:10.1016/S0048-9697(98)00341-6

Laschka, D., & Nachtwey, M. (1997). Platinum in municipal sewage treatment plants. *Chemosphere*, *34*(8), 1803–1812. doi:10.1016/S0045-6535(97)00036-2

López-Sánchez, D. E., Cobelo-García, A., Rijkenberg, M. J. A., Gerringa, L. J. A., & de

Baar, H. J. W. (2019). New insights on the dissolved platinum behavior in the Atlantic Ocean. *Chemical Geology*, *511*, 204–211. doi:10.1016/j.chemgeo.2019.01.003

Marques da Costa, E. (2016). Sócio-Economia. In J. Rocha (Ed.), *Atlas Digital da Área Metropolitana de Lisboa* (pp. 1–28). Lisboa, Portugal: Centro de Estudos Geográficos.

Mashio, A. S., Obata, H., & Gamo, T. (2017). Dissolved Platinum Concentrations in Coastal Seawater: Boso to Sanriku Areas, Japan. *Archives of Environmental Contamination and Toxicology*, *73*(2), 240–246. doi:10.1007/s00244-017-0373-1

Mashio, A. S., Obata, H., Tazoe, H., Tsutsumi, M., Ferrer i Santos, A., & Gamo, T. (2016). Dissolved platinum in rainwater, river water and seawater around Tokyo Bay and Otsuchi Bay in Japan. *Estuarine, Coastal and Shelf Science*, *180*, 160–167. doi:10.1016/j.ecss.2016.07.002

Meermann, B., & Nischwitz, V. (2018). ICP-MS for the analysis at the nanoscale – a tutorial review. *Journal of Analytical Atomic Spectrometry*, *33*(9), 1432–1468. doi:10.1039/C8JA00037A

Mil-Homens, M., Branco, V., Vale, C., Boer, W., Alt-Epping, U., Abrantes, F., & Vicente, M. (2009). Sedimentary record of anthropogenic metal inputs in the Tagus prodelta (Portugal). *Continental Shelf Research*, *29*(2), 381–392. doi:10.1016/j.csr.2008.10.002

Miller, J., & Miller, J. (2010). *Statistics and chemometrics for analytical chemistry* (6th ed.). Pearson Education Limited.

Monteiro, C. E., Cobelo-García, A., Caetano, M., & Correia dos Santos, M. (2020). Speciation analysis of Pt and Rh in urban road dust leachates. *Science of the Total Environment*, *722*, 137954. doi:10.1016/j.scitotenv.2020.137954

Monteiro, C. E., Cobelo-García, A., Caetano, M., & Correia dos Santos, M. M. (2017). Improved voltammetric method for simultaneous determination of Pt and Rh using second derivative signal transformation – application to environmental samples. *Talanta*, *175*, 1–8. doi:10.1016/j.talanta.2017.06.067

Monteiro, C. E., Correia dos Santos, M. M., Cobelo-García, A., Brito, P., & Caetano, M. (2019). Platinum and rhodium in Tagus estuary, SW Europe: sources and spatial distribution. *Environmental Monitoring and Assessment*, *191*(9), 579. doi:10.1007/s10661-019-7738-z

Neves, F. J. (2010). *Dynamics and hydrology of the Tagus estuary: results from in situ observations.* PhD Thesis, University of Lisbon, Portugal.

Neves, R. (1985). Biodimensional model for residual circulation in coastal zones: application to the Sado estuary. *Annales geophysicae*, *3*(4), 465–471.

Obata, H., Yoshida, T., & Ogawa, H. (2006). Determination of picomolar levels of platinum in estuarine waters: A comparison of cathodic stripping voltammetry and isotope dilution-inductively coupled plasma mass spectrometry. *Analytica Chimica Acta*, *580*(1), 32–38. doi:10.1016/j.aca.2006.07.044

Oun, R., Moussa, Y. E., & Wheate, N. J. (2018). The side effects of platinum-based chemotherapy drugs: a review for chemists. *Dalton Transactions*, *47*(19), 6645–

6653. doi:10.1039/C8DT00838H

Pawlak, J., Lodyga-Chruścińska, E., & Chrustowicz, J. (2014). Fate of platinum metals in the environment. *Journal of Trace Elements in Medicine and Biology*, *28*(3), 247–254. doi:10.1016/j.jtemb.2014.03.005

Peucker-Ehrenbrink, B., & Jahn, B. (2001). Rhenium-osmium isotope systematics and platinum group element concentrations: Loess and the upper continental crust. *Geochemistry, Geophysics, Geosystems*, *2*(10), n/a-n/a. doi:10.1029/2001GC000172

Rauch, S., & Peucker-Ehrenbrink, B. (2015). Sources of Platinum Group Elements in the Environment BT - Platinum Metals in the Environment. In F. Zereini & C. L. S. Wiseman (Eds.), (pp. 3–17). Berlin, Heidelberg: Springer Berlin Heidelberg. doi:10.1007/978-3-662-44559-4_1

Ravindra, K., Bencs, L., & Van Grieken, R. (2004). Platinum group elements in the environment and their health risk. *The Science of the total environment*, *318*(1–3), 1–43. doi:10.1016/S0048-9697(03)00372-3

Sung, W. (1995). Some Obsenmtions on Surface Partitioning of Cd, Cu, and Zn in Estuaries. *Environmental Science and Technology*, *29*(5), 1303–1312. doi:10.1021/es00005a024

Suzuki, A., Obata, H., Okubo, A., & Gamo, T. (2014). Precise determination of dissolved platinum in seawater of the Japan Sea, Sea of Okhotsk and western North Pacific Ocean. *Marine Chemistry*, *166*, 114–121. doi:http://dx.doi.org/10.1016/j.marchem.2014.10.003

Taylor, S. R., & McLennan, S. M. (1995). The geochemical evolution of the continental crust. *Reviews of Geophysics*, *33*(2), 241–265. doi:10.1029/95RG00262

Tessier, A. (2019). Sorption of Trace Elements on Natural Particles in Oxic Environments. In J. Buffle & H. P. van Leeuwen (Eds.), *Environmental Particles* (p. 576). CRC Press. doi:10.1201/9780429286223

Vale, C. (1986). Transport of particulate metals at different fluvial and tidal energies in the Tagus River estuary. *Rapports (Process Verbal) des Réunions du Conseil international pour l'Exploration de la Mer Méditerranée*, *186*, 306–312.

Vale, Carlos, & Sundby, B. (1987). Suspended sediment fluctuations in the Tagus estuary on semi-diurnal and fortnightly time scales. *Estuarine, Coastal and Shelf Science*, *25*(5), 495–508. doi:10.1016/0272-7714(87)90110-7

Vaz, N., & Dias, J. M. (2014). Residual currents and transport pathways in the Tagus estuary, Portugal: the role of freshwater discharge and wind. *Journal of Coastal Research*, 610–615. doi:10.2112/SI70-103.1

Vyas, N., Turner, A., & Sewell, G. (2014). Platinum-based anticancer drugs in waste waters of a major UK hospital and predicted concentrations in recipient surface waters. *Science of the Total Environment*, *493*, 324–329. doi:10.1016/j.scitotenv.2014.05.127

Wilkinson, K. J., & Lead, J. R. (2007). *Environmental Colloids and Particles: Behaviour, Separation and Characterisation*. (K. J. Wilkinson & J. R. Lead, Eds.)*Environmental Colloids and Particles: Behaviour, Separation and*

Characterisation (1st ed.). John Wiley & Sons, Ltd. doi:10.1002/9780470024539

Wolf, R. E., & Adams, M. (2015). *Multi-Elemental Analysis of Aqueous Geochemical Samples by ICP-MS*. doi:dx.doi.org/10.3133/ofr20151010

Zhong, L., Yan, W., Li, J., Tu, X., Liu, B., & Xia, Z. (2012). Pt and Pd in sediments from the Pearl River Estuary, South China: background levels, distribution, and source. *Environmental Science and Pollution Research*, *19*(4), 1305–1314. doi:10.1007/s11356-011-0653-7

Table 1 – Summary of concentrations found for Pt and Rh in particulate (Pt_P and Rh_P, respectively) and dissolved (Pt_D, $Pt_{D\text{-}ICP\text{-}MS}$ and Rh_D, respectively) fractions in ALC and VFX stations during neap tide (NT) and spring tide (ST).

		ALC - NT	***ALC - ST***	***VFX - NT***	***VFX - ST***
Pt_P	(ng g^{-1})	2.0-25.6	4.2-22.1	1.0-11.3	2.7-11.3
	(ng L^{-1})	0.03-0.64	0.3-1.3	0.08-0.71	0.13-0.28
Pt_D	(ng L^{-1})	0.2-5.3	0.2-11.7	0.18-0.43	0.12-0.73
$Pt_{D\text{-}ICP\text{-}MS}$	(ng L^{-1})	n.d.	n.d.	0.33-0.58	n.d.
Rh_P	(ng g^{-1})	0.3-5.1	0.2-4.3	0.1-2.0	0.2-1.8
	(ng L^{-1})	0.01-0.13	0.01-0.43	0.01-0.15	0.01-0.09
Rh_D	(ng L^{-1})	LOD*-0.12	LOD*-0.12	LOD*-0.05	LOD*-0.19

*n.d. - not determined; *LOD = 0.03 ng Rh L^{-1}*

Fig. 1 – Location of the sampling stations in the Tagus estuary, SW Europe. Imagery produced using MIRONE© software (Luis 2007) and bathymetric data obtained from the Portuguese Hydrographic Institute (http://www.hidrografico.pt). (The reader is referred to the web version of the article for the interpretation of color references.)

Fig. 2 – **a)** Particulate platinum (Pt_P) and rhodium (Rh_P) and **b)** dissolved platinum (Pt_D) and rhodium (Rh_D). in the water column at VFX station during neap tide (NT) and spring tide (ST) surveys. Tidal height – blue line; surface – white circles; bottom – black circles. The dotted line represents the limit of detection of Rh_D.

Fig. 3 – Platinum concentrations in the filtrates (<0.45 µm) measured by AdCSV (Pt_D; white circles) and ICP-MS ($Pt_{D\text{-}ICP\text{-}MS}$; orange circles) in the water column at VFX station during neap tide (NT). Tidal height – blue line. (The reader is referred to the web version of the article for the interpretation of color references.)

Fig. 4 – Concentrations of particulate (black circles) and dissolved (white circles) platinum (Pt_P and Pt_D, respectively) and rhodium (Rh_P and Rh_D, respectively) in the water column at ALC station during neap tide (NT) and spring tide (ST) surveys. Tidal height – blue line.

Fig. 5 – a) Distribution coefficients (K_D) along the conductivity gradient including both tidal cycles; **b**) Boxplot of the Log transformation of K_D for Pt and Rh in both stations monitored in the Tagus estuary.

Fig. 6 – Principal component analysis of data (particulate Pt – P-Pt; dissolved Pt – D-Pt; particulate Rh – P-Rh; dissolved Rh – D-Rh; temperature – T; conductivity – Cond; pH, dissolved oxygen – DO and %DO; and suspended particulate matter – SPM) obtained during neap tide (NT) and spring tide (ST) surveys for both ALC (blue circles) and VFX (red circles) stations. (The reader is referred to the web version of the article for the interpretation of color references.)

Fig. 7 – Projection of particulate and dissolved Pt and Rh concentrations on the current velocity (*u* component) obtained for ALC station. Blue boxes indicate the magnitude of the concentrations found for current velocities between 0.75 and 1.2 m s^{-1}.

Credit Author Statement

Carlos E. Monteiro: Conceptualization, Investigation, Writing - Original Draft, Review & Editing, Visualization.

Antonio Cobelo-García: Conceptualization, Investigation, Writing - Original Draft, Review & Editing, Visualization.

Margarida Correia dos Santos: Conceptualization, Writing - Original Draft, Review & Editing, Visualization.

Miguel Caetano: Conceptualization, Writing - Original Draft, Review & Editing, Visualization, Funding acquisition, Supervision.

Declaration of interest

The authors declare that they have no known competing financial interests or personal relationships that could have appeared to influence the work reported in this paper.

Highlights

- Particulate and dissolved Rh concentrations were determined in an estuary
- Sources of Pt in wastewater from anticancer therapy and domestic sewage
- Pt speciation analysis in the water column <0.45 µm was shown
- Particle–water interactions of Rh and Pt did not vary with the salinity gradient
- Estuaries are an important pathway for PGE to be transferred to the ocean

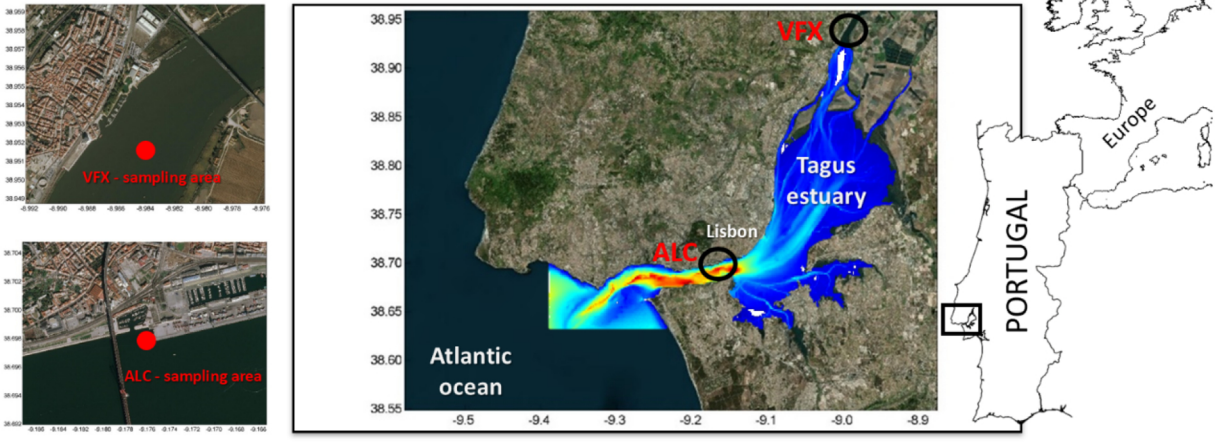
VFX - sampling area
ALC - sampling area
VFX
Tagus estuary
Lisbon
ALC
Atlantic ocean
38.95
38.90
38.85
38.80
38.75
38.70
38.65
38.60
38.55
-9.5
-9.4
-9.3
-9.2
-9.1
-9.0
-8.9
Europe
PORTUGAL

Figure 1

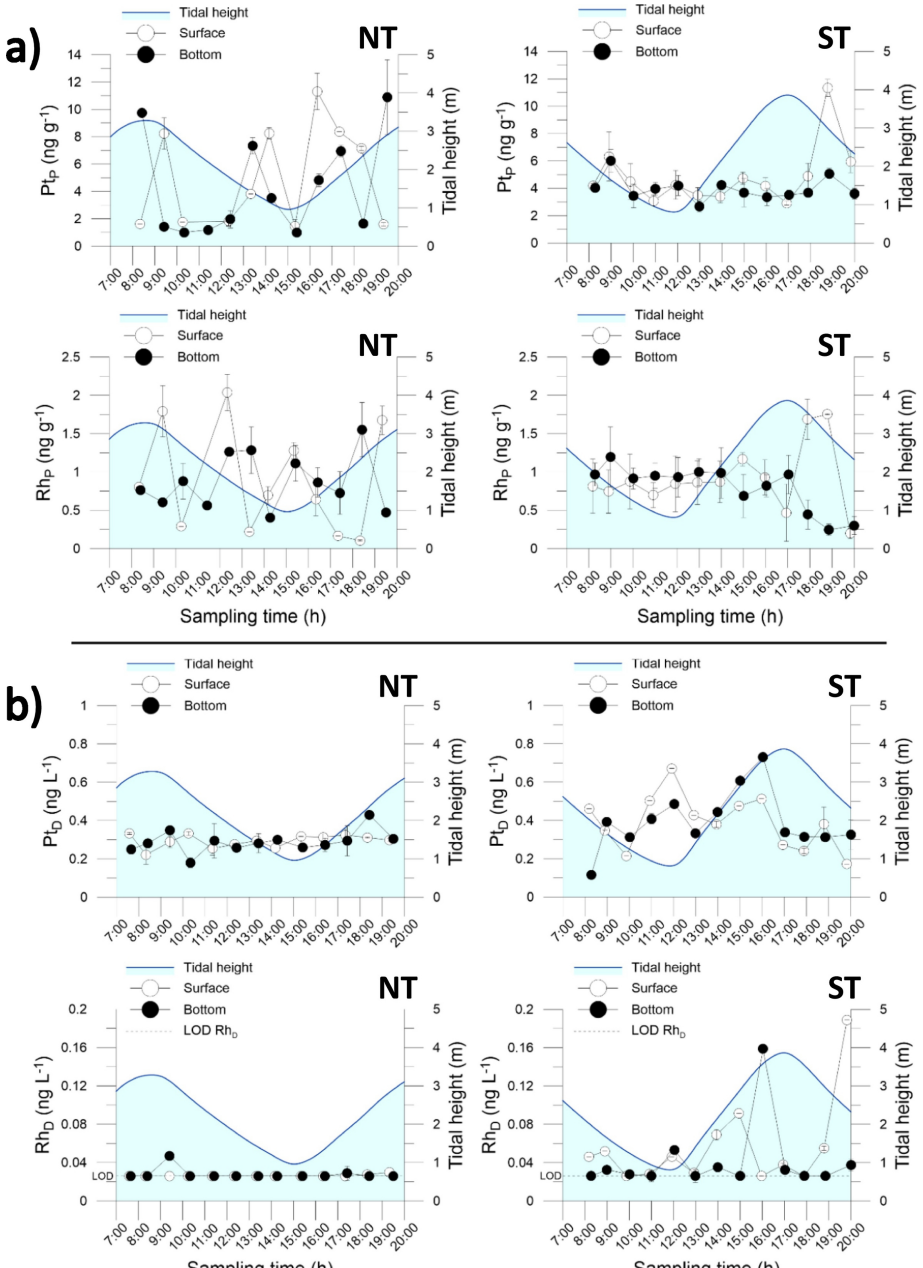
a)
NT
ST
Tidal height
Surface
Bottom
Pt_P (ng g^{-1})
Rh_P (ng g^{-1})
Tidal height (m)
Sampling time (h)
b)
Pt_D (ng L^{-1})
Rh_D (ng L^{-1})
LOD Rh_D
LOD

Figure 2

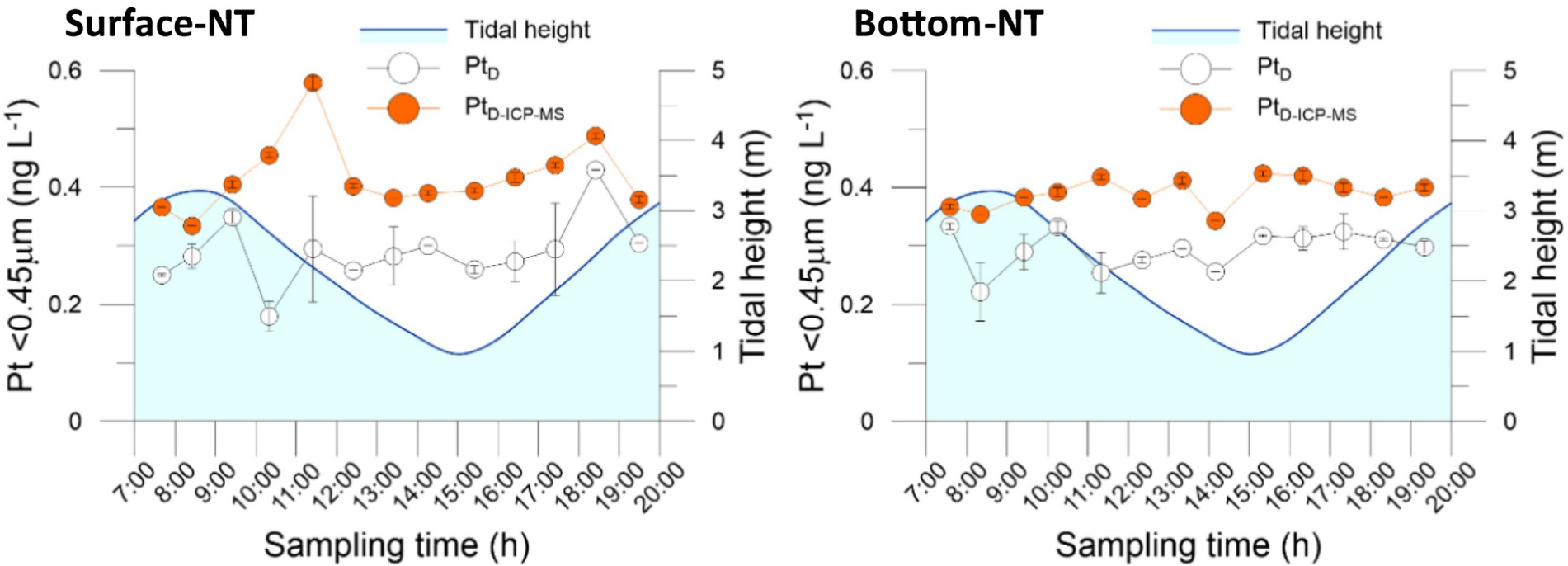
Surface-NT
Tidal height
Pt_D
$Pt_{D\text{-}ICP\text{-}MS}$
Pt <0.45µm (ng L^{-1})
Tidal height (m)
Sampling time (h)
Bottom-NT
Tidal height
Pt_D
$Pt_{D\text{-}ICP\text{-}MS}$
Pt <0.45µm (ng L^{-1})
Tidal height (m)
Sampling time (h)

Figure 3

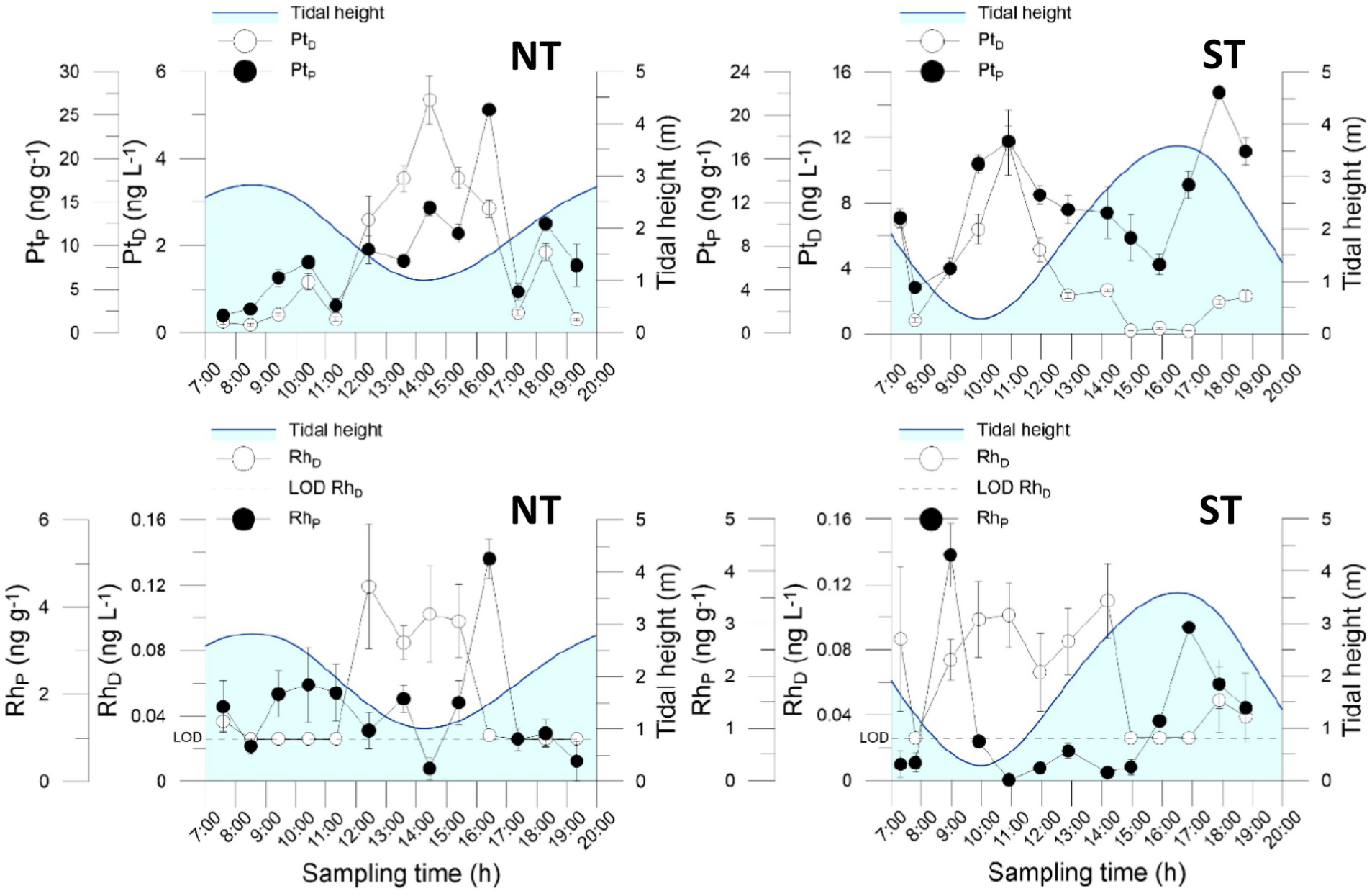
NT
ST
Tidal height
Pt_D
Pt_P
Rh_D
LOD Rh_D
Rh_P
Pt_P (ng g^{-1})
Pt_D (ng L^{-1})
Rh_P (ng g^{-1})
Rh_D (ng L^{-1})
Tidal height (m)
LOD
Sampling time (h)

Figure 4

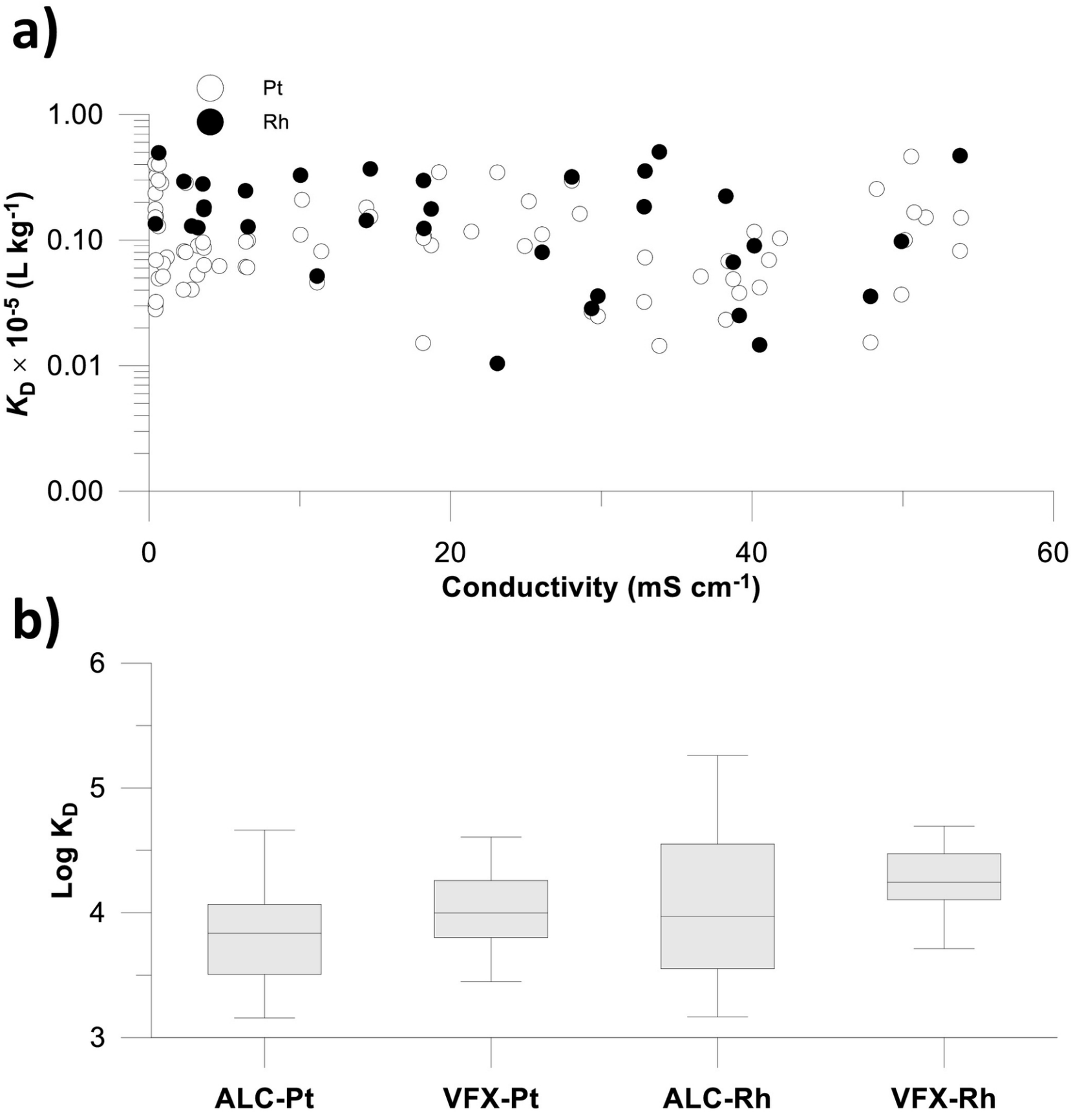
a)
Pt
Rh
1.00
0.10
0.01
0.00
$K_D \times 10^{-5}$ (L kg^{-1})
0
20
40
60
Conductivity (mS cm^{-1})
b)
6
5
4
3
Log K_D
ALC-Pt
VFX-Pt
ALC-Rh
VFX-Rh

Figure 5

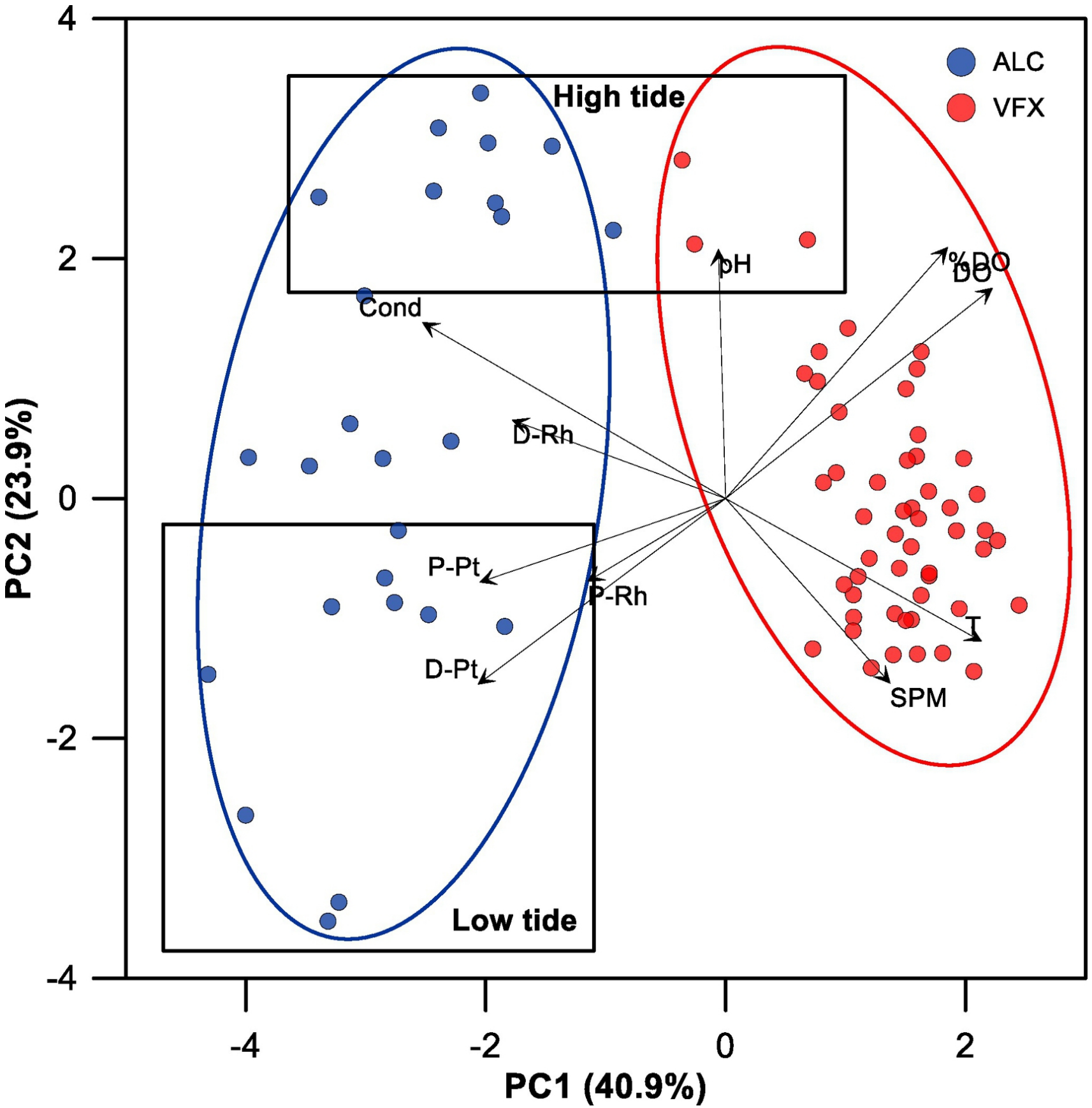
ALC
VFX
High tide
Low tide
pH
%DO
DO
Cond
D-Rh
P-Pt
P-Rh
D-Pt
T
SPM
PC1 (40.9%)
PC2 (23.9%)
4
2
0
-2
-4
-4
-2
0
2

Figure 6

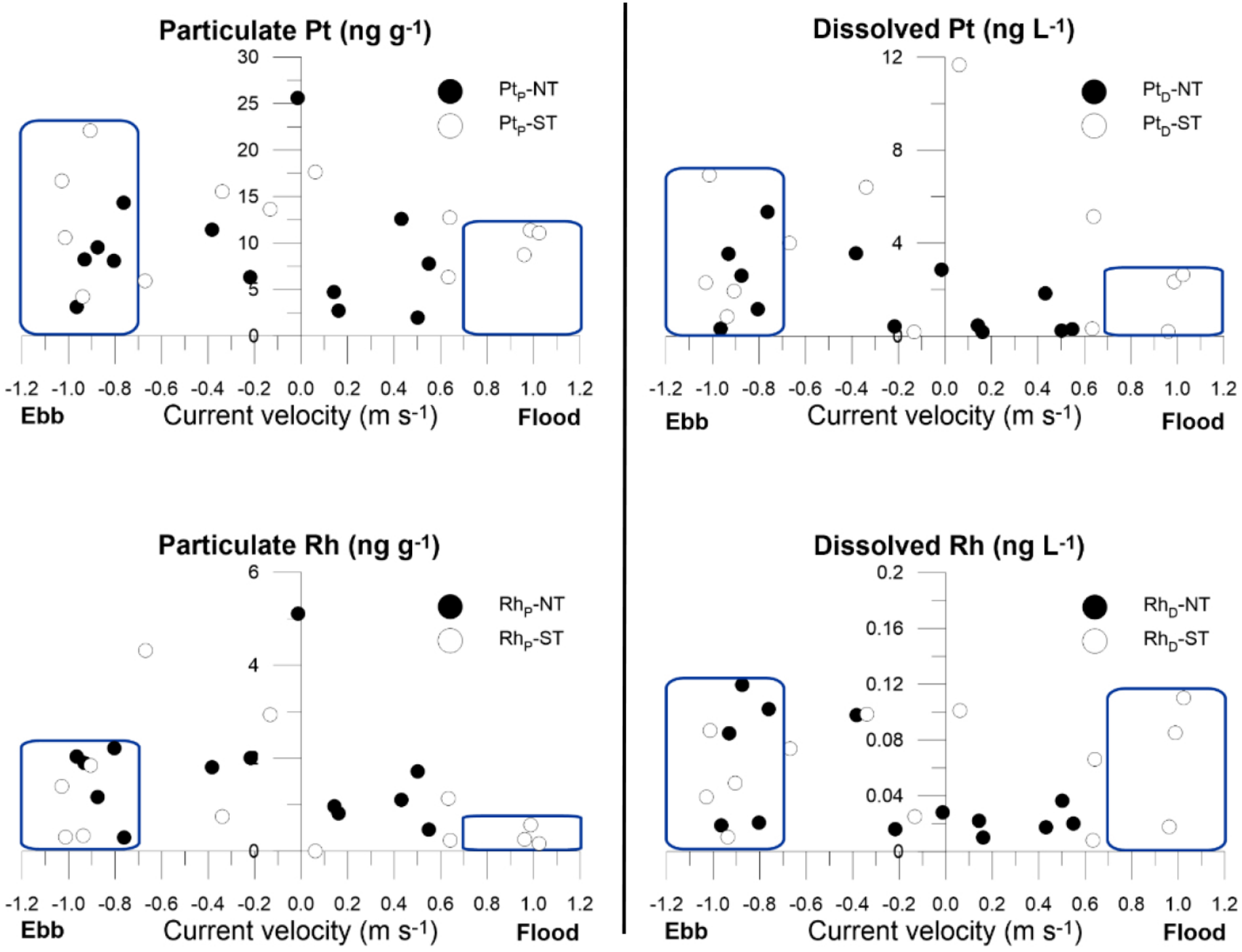
Particulate Pt (ng g-1)
Pt_P-NT
Pt_P-ST
Dissolved Pt (ng L-1)
Pt_D-NT
Pt_D-ST
Particulate Rh (ng g-1)
Rh_P-NT
Rh_P-ST
Dissolved Rh (ng L-1)
Rh_D-NT
Rh_D-ST
Ebb
Current velocity (m s-1)
Flood

Figure 7